DNA-TR-81-35

# LATE DUST PEDESTAL RISE MECHANISMS

D. H. Sowle
R. H. Christian
Mission Research Corporation
P.O. Drawer 719
Santa Barbara, California 93102



31 August 1981

Technical Report

CONTRACT No. DNA 001-81-C-0162

APPROVED FOR PUBLIC RELEASE;
DISTRIBUTION UNLIMITED.

THIS WORK SPONSORED BY THE DEFENSE NUCLEAR AGENCY
UNDER RDT&E RMSS CODE B345081466 J11AAXAX00007 H2590D.



Prepared for
Director
DEFENSE NUCLEAR AGENCY
Washington, D. C. 20305

BLANK PAGES
IN THIS
DOCUMENT
WERE NOT
FILMED

Destroy this report when it is no longer needed. Do not return to sender.

PLEASE NOTIFY THE DEFENSE NUCLEAR AGENCY, ATTN: STTI, WASHINGTON, D.C. 20305, IF YOUR ADDRESS IS INCORRECT, IF YOU WISH TO BE DELETED FROM THE DISTRIBUTION LIST, OR IF THE ADDRESSEE IS NO LONGER EMPLOYED BY YOUR ORGANIZATION.

UNCLASSIFIED

SECURITY CLASSIFICATION OF THIS PAGE *(When Data Entered)*

| REPORT DOCUMENTATION PAGE | | READ INSTRUCTIONS BEFORE COMPLETING FORM |
|---|---|---|
| 1 REPORT NUMBER<br>DNA-TR-81-35 | 2. GOVT ACCESSION NO.<br>AD-A113 112 | 3. RECIPIENT'S CATALOG NUMBER |
| 4 TITLE *(and Subtitle)*<br>LATE DUST PEDESTAL RISE MECHANISMS | | 5. TYPE OF REPORT & PERIOD COVERED<br>Technical Report |
| | | 6. PERFORMING ORG. REPORT NUMBER<br>MRC-R-657 |
| 7 AUTHOR(s)<br>D. H. Sowle<br>R. H. Christian | | 8 CONTRACT OR GRANT NUMBER(s)<br>DNA 001-81-C-0162 |
| 9 PERFORMING ORGANIZATION NAME AND ADDRESS<br>Mission Research Corporation<br>P.O. Drawer 719<br>Santa Barbara, California 93102 | | 10 PROGRAM ELEMENT, PROJECT, TASK AREA & WORK UNIT NUMBERS<br>Subtask J11AAXAX000-07 |
| 11 CONTROLLING OFFICE NAME AND ADDRESS<br>Director<br>Defense Nuclear Agency<br>Washington, D.C. 20305 | | 12 REPORT DATE<br>31 August 1981<br>13 NUMBER OF PAGES<br>34 |
| 14 MONITORING AGENCY NAME & ADDRESS*(if different from Controlling Office)* | | 15. SECURITY CLASS *(of this report)*<br>UNCLASSIFIED<br>15a. DECLASSIFICATION DOWNGRADING SCHEDULE<br>N/A |

16 DISTRIBUTION STATEMENT *(of this Report)*

Approved for public release; distribution unlimited.

17 DISTRIBUTION STATEMENT *(of the abstract entered in Block 20, if different from Report)*

18 SUPPLEMENTARY NOTES

This work sponsored by the Defense Nuclear Agency under RDT&E RMSS Code B345081466 J11AAXAX00007 H2590D.

19 KEY WORDS *(Continue on reverse side if necessary and identify by block number)*

Nuclear Lofted Dust Clouds
Dust Pedestal

20 ABSTRACT *(Continue on reverse side if necessary and identify by block number)*

The mechanism of buoyant rise is found to be quantitatively consistent with readily available photographic data on the late dust pedestal of events Wasp Prime and Climax. The term "late" refers to times after the rapid initial pedestal rise, and can be conveniently defined in terms of Liner's model.[1] One implication of buoyancy as a driving force for late pedestal rise is that the average bulk density in most or all of the dust pedestal is small compared to air density, that is, small compared to $10^{-3}$ g/cm$^3$.

DD FORM 1 JAN 73 1473 EDITION OF 1 NOV 65 IS OBSOLETE

UNCLASSIFIED

SECURITY CLASSIFICATION OF THIS PAGE *(When Data Entered)*

20. ABSTRACT (continued)

A number of mechanisms other than buoyancy were investigated as causes for the late rise with discouraging results; these mechanisms are listed along with a brief description of the reasons each is untenable.

# PREFACE

Major Leon A. Wittwer, USAF, brought the possibility of buoyancy as a driving force to our attention, based upon the resemblence between a late dust pedestal and the top of a layer of summer cumulus clouds.

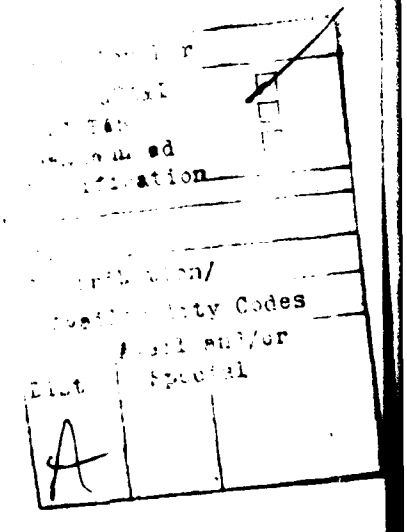

TABLE OF CONTENTS

LIST OF TABLES

# SECTION 1
# INTRODUCTION AND SUMMARY

A rapid survey of available literature and data was undertaken in an attempt to become familiar with the state of understanding of the dust pedestal, and to determine if any areas of phenomenology appeared ripe for pursuit, particularly matters which might contribute to electromagnetic propagation interference understanding. We quickly became engrossed in the mysteries of the nearly rectangular vertical profile of the pedestal, its sharp edge, long continuing rise, near universal occurrence over a wide range of conditions, and other phenomena more minor in impact and less universal in occurrence, but equally mystifying, such as the marvelous central sand column of some events. This report documents results of our efforts to understand only one of the above aspects of the pedestal, the lofting mechanism for its late slow rise. As an accidental byproduct of this investigation, the rise rate of the sand column, but not its existence, is explained.

Section 2 explains the terminology of those aspects of the dust pedestal which concern us.

In Section 3 it is shown that at late times a rather steady excess velocity, nearly vertical, is present in the flow field in addition to that anticipated due to the rising fireball or its shocks and rarefactions; at least this is so in the two cases investigated to date. These are Wasp Prime (3.2 KT at 225 m) and Climax (61 KT at 407 m). These shots were chosen for the initial study for two reasons: (1) burst height was low enough to raise a dust pedestal but high enough not to create a crater which would confuse data with ejecta, and (2) data on these two shots were readily available, in excellent pictures with accompanying dimensional information.[2a,b]

In Section 4 it is shown that excess rise velocities measured for identifiable features at the top of the dust pedestal are reasonably consistent with theoretical estimates based on buoyancy estimates and measured feature size.

From consistency of buoyancy as a driving mechanism follows the conclusion that at least at late times in the buoyant portion of the pedestal, bulk dust density must be too low to seriously interfere with the force balance. These forces are estimated to be caused by 5 percent to 50 percent air density depletion due to thermal expansion. Accordingly, dust bulk density must be less than 5 percent to 50 percent of air density.

Examination of the photographs show the features on which this low dust density conclusion is based to be comparable to the pedestal thickness in dimension. This implies local "buoyant thermal" or vortex flow fields which extend throughout the vertical thickness of the pedestal. Thus is implied, although not with the strength of the dust density limit above, that this limit on bulk density extends throughout most, if not all of the pedestal.

Calculations of Gutsche,[3] Lauer,[4] and Thompson[5] show that at such low levels of dust density the radar propagation problem is reduced to one of angular scintillation; signal blackout cannot be overriding. Scaling to probable threat level yield is problematical at the moment, although the required extrapolation in yield is no greater than that between the two events here investigated—and bulk density has the same limit for these cases.

Finally, Section 5 outlines considerations which lead to rejection of a short list of candidate phenomena as causes of the late dust rise. Most or all of these phenomena may, in fact, occur but none seems adequate singly or in concert to do more than initiate a low dust cloud. Some other

mechanism must raise it rapidly during the early phase in preparation for the buoyant late phase.

## SECTION 2
## TERMINOLOGY

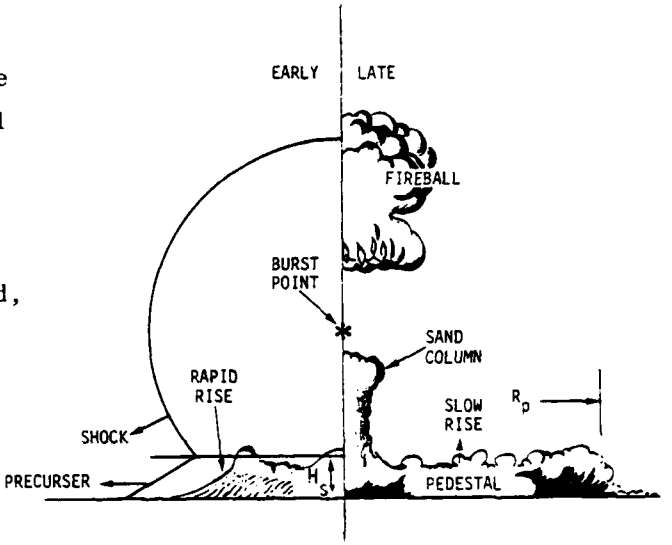


A qualitative outline of the early, formative stage of the pedestal is illustrated on the left of the sketch. The dust cloud rises immediately behind the shock, or the precursor, if present. The rise is rapid, typically at velocities of tens to hundreds of meters per second until height $H_s$ is reached within a second of shock passage. After this time the rise rapidly slows, by about an order of magnitude, but continues for a long time: minutes. The slowing in rise velocity is so abrupt that Liner, et al.[1] have modeled the rise velocity as discontinuous at $H_s$. Very roughly,

$$H_s \sim 100\ [Y(MT)]^{1/3} \quad \text{meters} \quad . \tag{1}$$

Prior to reaching $H_s$, dust laden material rises at a rate of order

$$v_- \sim \text{hundreds of meters/sec} \quad , \tag{2}$$

after reaching $H_s$, material slows to

$$v_+ \sim \text{tens of meters/sec} \tag{3}$$

and continues to rise for several minutes; presumably it gradually slows to a stop. None of the above numbers should be taken as accurate; see Reference 1 for one set of self consistent parameter values.

An approximation to the above behavior occurs without radial dependence other than timing out to the maximum pedestal radius, $R_p$, which is typically at a distance of two to three fireball radii from ground zero. Time starts counting when the shock or its precursor reaches a given point. Actually, many believe that $H_s$ increases with distance from ground zero out to $R_p$, where the process of pedestal creation abruptly ceases.

The late pedestal, shown on the right of the sketch, is characterized by a very uneven top surface composed of more or less random lumps with apparent outer scale size about equal to pedestal height. Many lumps in this structure can be identified in successive frames of motion pictures; thus their development and motion can be followed for analysis.

An exception to the random structure is the so called sand column. This feature is observed for burst heights greater than a fireball radius (of course it would be invisible at lower heights) and less than two or three fireball radii. The sand column is aptly named; it appears to be a column of dirt which forms at ground zero promptly after the shock strikes. Its radius is about half that of the fireball and remains roughly constant in time. The sand column shoots upward as a cylinder, eventually overtaking the fireball and taking on the appearance of a classic mushroom cloud stem, albeit a bit narrower stem than usual. We draw attention to it here because, despite its extraordinary appearance, its motion appears to be due to the same forces which control the remainder of the late dust pedestal.

## SECTION 3
## DEMONSTRATION OF EXCESS VERTICAL PEDESTAL VELOCITY

### QUIESCENT FLOW

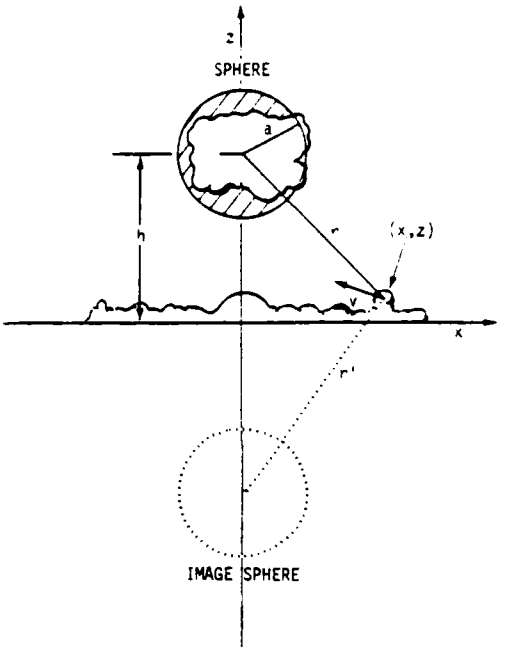


Under ideal conditions, after the shock has gone and its reverberations calmed, the flow field exterior to the fireball should be predictable from the rising motion of the fireball. The dominant motion at position, r, should be the sum of that due to a dipole field exterior to a rising sphere of radius, a, adequate to encompass the fireball or perhaps a bit larger and, because the ground surface is impenetrable, an image dipole below the ground. These spheres and their relation to an observation point at (x,z) are shown in the sketch.

If the fireball, represented by a sphere of radius, a, rises through an element of height, dh, then the material at (x,z) should be displaced by

$$dx = \frac{3a^3 x}{2} \left[ (h-z)/r^5 + (h+z)/r'^5 \right] dh \qquad (4)$$

$$dz = a^3 \left| \left[ (h-z)^2 - x^2/2 \right]/r^5 - \left| (h+z)^2 - x^2/2 \right|/r'^5 \right| dh \qquad (5)$$

where $r^2 = (h-z)^2 + x^2$ and $(r')^2 = (h+z)^2 + x^2$ . (6)

If one wishes to analyze the motion of a feature visible on a photograph, it is not certain that the feature is in the plane which passes through the burst point perpendicular to the observer. In that case, one must assume a value of azimuth angle, $\phi$ and set

$$x = x_a/\cos\phi \tag{7}$$

where $x_a$ is the "apparent" or projected value of $x$. The equation of motion for the apparent $x$ is obtained by multiplying the right hand side of (4) by $\cos\phi$.

Attempts to match the observed motion of lumps in the Wasp Prime and Climax late dust pedestals to these simple flows were unsuccessful, the observed vertical motion being significantly greater than expected.

## EXCESS VELOCITY

To investigate the effect of a possible excess vertical velocity, a term is added to Equation 5 for $dz$.

$$dz_e = u\,dt = u(dt/dh)dh = u/U\,dh \tag{8}$$

where $u$ is the excess velocity and $U$ is fireball rise velocity.

## WASP PRIME DATA

Wasp Prime was a 3.2 KT air drop exploded at 225 meters above the Nevada Proving Grounds as event 9 of Operation Teapot.

Features identifiable in successive plates of Dudziak's report[2a] were measured by hand directly from the report. The (x,z) trajectories measured for these features are shown in Table 1 and Figure 1, which also shows the fireball center location and fireball radius. Feature number 3

Table 1. Measured feature trajectories for Wasp Prime. Trajectories measured from west station photos in Ref. 2a are shown for five features. Feature 3 is the sand column, feature 2 is known to have $\phi$=0. The first column has time in seconds post shot. Coordinates x and z are apparent Cartesian coordinates in meters, projected into the photographic plane. Note that features 1 and 2 are at negative values of x.

| | Feature 1 | | Feature 2 | | Feature 3 | | Feature 4 | | Feature 5 | |
|---|---|---|---|---|---|---|---|---|---|---|
| t(sec) | -x | z | -x | z | x | z | x | z | x | z |
| 1.005 | | | | | | | | | 222.3 | 12 |
| 1.095 | | | | | | | | | 222.8 | 11 |
| 1.298 | | | | | | | | | 218.8 | 13 |
| 1.503 | 124.2 | 19 | | | | | 130.8 | 15 | 210.8 | 13 |
| 1.698 | 122.3 | 20 | | | | | 133.7 | 18 | 207.7 | 17 |
| 1.903 | 120.3 | 22 | 80.3 | 18 | | | 131.7 | 20 | 203.7 | 19 |
| 2.001 | 120.8 | 22 | 76.8 | 19 | 0 | 55 | 131.2 | 20 | 205.2 | 19 |
| 2.205 | 119.4 | 23 | 74.4 | 22 | | | 127.6 | 20 | 205.6 | 20 |
| 2.400 | 118.1 | 26 | 75.1 | 25 | | | 127.9 | 23 | 206.9 | 22 |
| 2.498 | 116.2 | 28 | 74.2 | 26 | | | 127.8 | 25 | 204.8 | 24 |
| 2.700 | 114.1 | 28 | 72.2 | 27 | | | 127.8 | 26 | 206.8 | 24 |
| 2.904 | 115.4 | 29 | 72.4 | 27 | | | 123.6 | 27 | 202.6 | 25 |
| 3.002 | 113.0 | 30 | 69.0 | 28 | 0 | 95 | 125.0 | 28 | 204.0 | 26 |
| 3.099 | 112.0 | 31 | 71.0 | 30 | | | 125.0 | 30 | 204.0 | 25 |
| 3.505 | 110.1 | 32 | 71.1 | 32 | | | 122.9 | 28 | 200.9 | 25 |
| 3.807 | 108.7 | 33 | 69.7 | 35 | | | 120.3 | 29 | 200.3 | 26 |
| 4.008 | 104.8 | 37 | 64.8 | 39 | 0 | 132 | 124.2 | 30 | 203.2 | 27 |
| 4.25 | 100.7 | 35 | 65.7 | 40 | | | 121.3 | 30 | 201.3 | 28 |
| 4.50 | 100.7 | 37 | 67.7 | 42 | | | 119.3 | 31 | 199.3 | 28 |
| 4.75 | 97.8 | 40 | 65.8 | 45 | | | 119.2 | 33 | 202.2 | 28 |
| 5.00 | 99.8 | 40 | 67.8 | 47 | 0 | 175 | 116.2 | 33 | 197.2 | 30 |
| 5.50 | | | | | | | 117.1 | 33 | 195.1 | 30 |
| 6.00 | | | | | | | 118.7 | 35 | 198.7 | 34 |
| 6.50 | | | | | | | 120.6 | 37.5 | 195.6 | 33 |

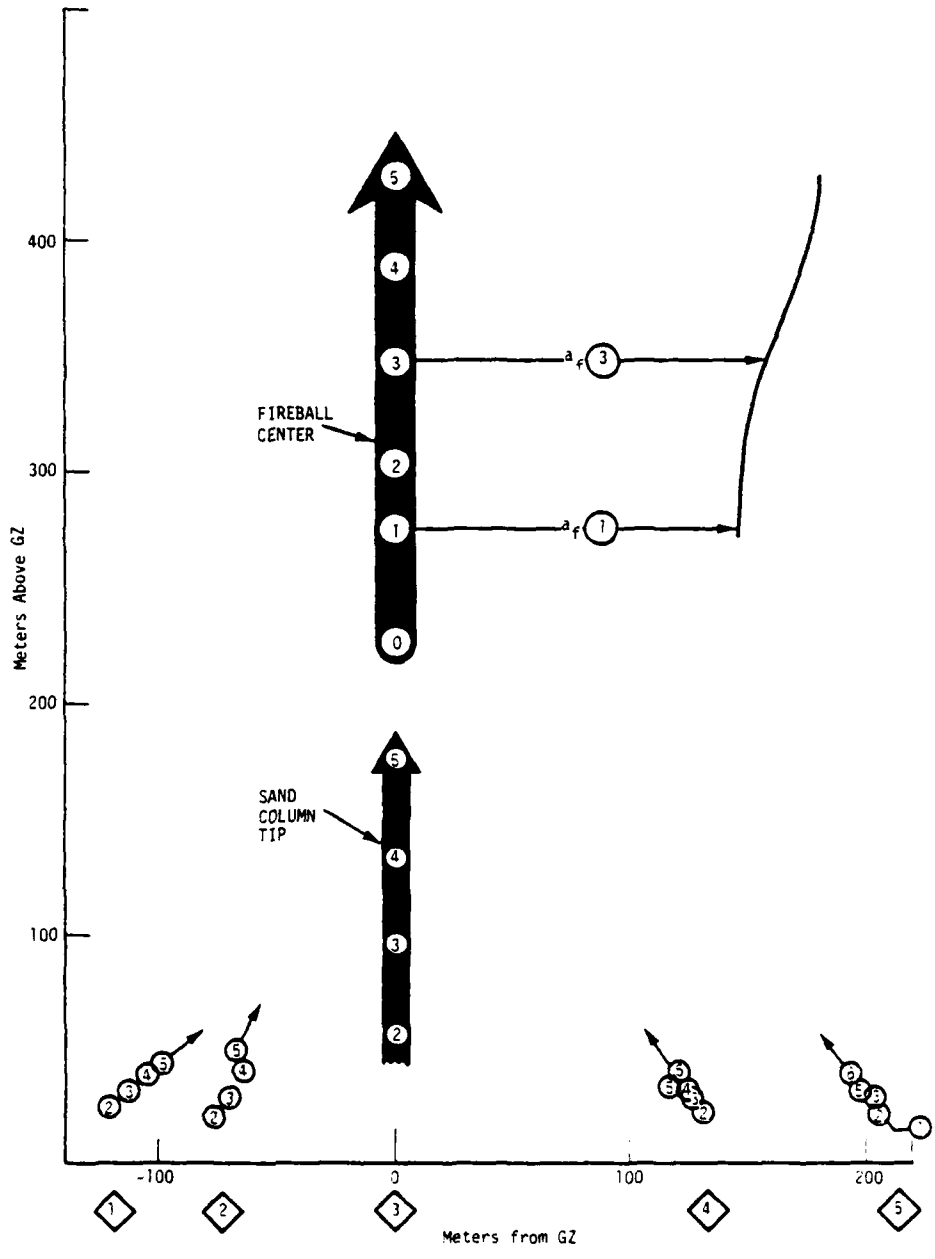


Figure 1. Motion of Wasp Prime features, as measured from Ref. 2a. Encircled integers are times in seconds when the features, identified numerically in diamonds below the horizontal axis, were located at circle centers. The quantity $a_f$, is apparent horizontal fireball radius.

is the top of the sand column. Feature number 2 is identifiable from the north station as well as the west station and, as viewed from west station, has $\dot{\phi} = 0$. The apparently erratic motion of the features is not believed to be real, but rather is due to crude measuring techniques; nevertheless, the trend of motion should be reliable.

Later we will have need of the characteristic radius of each feature. Approximate values measured during the observation interval are shown in Table 2.

Table 2. Characteristic radii of Wasp Prime features.

| Feature | 1 | 2 | 3 | 4 | 5 |
|---|---|---|---|---|---|
| Radius (m) | 5.9 | 4.4 | 44.0 | 5.9 | 7.3 |

## RESULTS OF WASP PRIME COMPARISON

Equations 4 through 8 were entered into a computer, along with an interpolated tabular fit to fireball center position, h, and radius, $a_f$. A number of ratios of equivalent sphere radius, a, to horizontal fireball radius, $a_f$, were attempted. The quality of obtainable fits to the five observed features deteriorated markedly for $a/a_f$ outside the range

$$1.2 \lesssim a/a_f \lesssim 1.3 \quad . \tag{9}$$

This range is determined basically by the change in x over the observation time. Smaller values of $a/a_f$ gave estimates of motion too small and larger values gave estimates too large. Our first conclusion, then, is that the effective value of radius for the volume of air moving with the fireball is 1.2 to 1.3 times the observed horizontal fireball radius.

The second conclusion reached is that significant upward velocites in excess of that due to the ideal flow field are necessary for each feature. The best time averaged value of excess velocity, u, is listed for each feature in Table 3, taking the mean fireball rise velocity during the period of observation to be 40 m/sec.

Best fits for features 4 and 5 occur at values of $\cos\phi$ of 0.7 to 0.8, while $\cos\phi = 1.0$ worked best for the others.

Table 3. Wasp Prime excess velocities

| Feature | | 1 | 2 | 3 | 4 | 5 |
|---|---|---|---|---|---|---|
| u | $a/a_f$=1.2 | 3.2 | 4.8 | 22. | 4.0 | 4.8 |
| (m/s) | $a/a_f$=1.3 | 4.0 | 5.6 | 18. | 4.4 | 4.8 |

CLIMAX DATA

Climax was a 61 kt air drop exploded 407 meters above the Nevada Proving Ground as event 11 of series Upshot-Knothole. It was one of the largest yield devices ever tested over the Nevada Proving Ground. The scaled height of burst ($Y^{1/3}$) is about two-thirds that of event Wasp Prime.

Experience with Wasp Prime showed that most of the vertical motion was in fact considerably in excess of that due to an ideal flow field. Thus elaborate computations of dipole and image dipole flow fields were not really necessary to extract an approximate value of excess vertical velocity. Only a fairly small correction for the effect of the dipole fields is necessary. Accordingly, values of observed upward velocities for event Climax were corrected for ideal flow field effects by factors found in analysis of Wasp Prime data. For all points other than the sand column, 80 percent of the observed velocity was taken to be excess. For the sand column, 45 percent of observed velocity was taken to be excess.

A summary of Climax features that were analyzed based on photographic data and scales provided in Reference 2b appears in Table 4.

Table 4. Climax data. The first column is feature identification, the second column approximate feature horizontal location, x(m) at about 8 seconds post shot as viewed from the west station. The third and fourth columns show the observed total velocity, $V_z$(m/s), and the estimated excess upward velocity, u(m/s). The fifth column is the feature's characteristic radius in meters. Feature 3 is the sand column.

| Feature | x(m) | $V_z$(m/s) | u(m/s) | R(m) |
|---|---|---|---|---|
| 1 | -600 | 10.7 | 8.6 | 36 |
| 2 | -350 | 15.9 | 12.7 | 55 |
| 3 | 0 | 80.0 | 36.0 | 128 |
| 4 | 800 | 10.0 | 8.0 | 30.3 |

# SECTION 4
# COMPARISON OF EXCESS RISE VELOCITY DATA TO THAT EXPECTED FROM BUOYANCY

Consideration of the general appearance of a late pedestal and of the amount of energy striking the area as thermal radiation or shock leads one to suspect that the dust pedestal may be buoyant due to thermal expansion of heated air, unless in fact the air is so laden with dust as to overpower this buoyancy. In order to investigate this possibility, a comparison of the excess rise velocity observed for individual features can be made to that expected for buoyantly driven rise.

As a preliminary observation, note that the density of dust necessary to record photographically is relatively small and comes almost entirely from the finest dust particles in the distribution. For example, dust density of the order of $10^{-5}$ to $10^{-6}$ gm/cm$^3$ consisting of 10 micron particles, too thin to interfere seriously with many radio or radar frequencies, would be sufficient to record on film as an opaque cloud.

## EXPECTED RISE RATE OF OUTSTANDING LUMPS

If the pedestal material rises because dust in combination with warmed, expanded air is buoyant then the objects measured, which must strongly protrude to be observable, should behave roughly as rising hot air "thermals" or buoyant spheres.

An estimate of the buoyant rise velocity may be obtained by equating the buoyant force to the drag force and solving for the quasi-steady velocity. The buoyant force, by Archimedes principle, is the difference between the weight of the displaced fluid and the weight of the body. For

this purpose we assume a spherical bubble of radius R,

$$F_b = \frac{4\rho}{3} R^3(\rho_a - \rho)g \tag{10}$$

where $\rho_a$ is the density of ambient air, $\rho$ is the (average) density of the bubble, and $g$ is gravitational acceleration.

The drag force of an object of cross sectional area, $\pi R^2$, moving at a velcoity, u, is by definition,

$$F_d = C_D \rho_a \frac{u^2}{2} (\pi R^2) \tag{11}$$

where the drag coefficient is a function of body shape and Reynolds number. We will use a value of $C_D = 0.6$, appropriate to a smooth sphere in high Reynolds number, laminar flow.* Equating these forces and solving for u yields

$$u = \left[\frac{8}{3C_D} g R \frac{\Delta\rho}{\rho_a}\right]^{1/2} \approx 2.1\sqrt{g R \Delta\rho/\rho_a} , \tag{12}$$

where $\Delta\rho = \rho_a - \rho$. This quasi-equilibrium estimate neglects impulsive forces[6] necessary during the initiation of the motion and therefore is an upper limit.

The smallest likely rise rate may be obtained by extrapolating a formula due to McCartor and Wortman.[7] For the early rise rate of a perfect, spherical, hollow bubble in quiescent air they find

$$u \approx 0.8\sqrt{gR} . \tag{13a}$$

To account for the actual, but relatively low, density of the pedestal features we modify their formula to include the relative density, i.e.,

$$u = 0.8\sqrt{gR\Delta\rho/\rho_a} . \tag{13b}$$

*The decrease in $C_D$ that occurs for a solid sphere at Reynolds number greater than $10^4$ is due to detachment. For underdense gas spheres, this seems unlikely to us.

From the above two limits we conclude that buoyant forces should lead to a feature rise velocity in the range

$$0.8 \lesssim \frac{u}{\sqrt{gR\Delta\rho/\rho_a}} \lesssim 2.1 \quad . \tag{14}$$

ESTIMATE OF $\Delta\rho/\rho_a$

Ganong and Whitaker[8] use several empirical but reasonable formulae in an attempt to match air temperature measurements near the surface following explosions of the Tumbler series, and also to match the precursor shock behavior of shot Priscilla. Based on comparison of these several formulae to data, an appropriate formula for bomb thermal radiation which is deposited in air as thermal energy, $\varepsilon$, appears to be

$$\varepsilon = \frac{f_c f_r W h}{4\pi r^3} \tag{15}$$

where $f_c$ is bomb thermal to air thermal coupling fraction, $f_r$ is bomb thermal radiation fraction, $W$ is total yield, $h$ is burst height above ground zero, and $r$ is the distance from burst point to surface, approximately

$$r = (h^2 + x^2)^{1/2} \tag{16}$$

where as before, $x$ is horizontal distance from ground zero. Ganong and Whitaker found best agreement with precursor data in our range of $x$ for $f_c = 1/6$.

Equation 15 provides a means of estimating the energy deposited per unit area. It is then necessary to discover, or guess, how this energy mixes vertically into a volume which must eventually expand to pressure equilibrium with the ambient atmosphere. All evidence points out to very rapid initial mixing as evidenced by the fast initial rise of the pedestal. Leaning heavily on this sparce evidence, we assume the energy deposited

in some area to be uniformly mixed vertically to a height, $\ell_o$, so quickly that no net work is done on the exterior during this expansion via mixing, thus no energy is lost.

The resultant mix of air at ambient density and uniform super-ambient temperature is then assumed to expand adiabatically to pressure equilibrium.

When energy $\varepsilon$ per unit area is distributed in air to height, $\ell_o$, at ambient density, $\rho_a$, the air specific internal energy will be

$$I_o = \frac{\varepsilon}{\ell_o \rho_a} + I_a \tag{17}$$

where $I_a$ is ambient specific internal energy,

$$I_a = \frac{p_a}{(\gamma-1)\rho_a} \tag{18}$$

where $\gamma$ is the normal air polytropic constant.

Then, substituting (18) into (17), the raised pressure, $p_o$, will be given by

$$\frac{p_o}{p_a} = \frac{I_o}{I_a} = 1 + \frac{(\gamma-1)\varepsilon}{\ell_o p_a} \tag{19}$$

and, after adiabatic expansion back to ambient pressure, $p_a$, the density will be given by

$$\frac{\rho}{\rho_a} = \left(\frac{p_o}{p_a}\right)^{1/\gamma} = \left[1 + \frac{(\gamma-1)\varepsilon}{\ell_o p_a}\right]^{1/\gamma} \tag{20}$$

but, since expansion is almost entirely one dimensional in the vertical direction, raising material at height $\ell_o$ to the pedestal height, $H_s$, at the end of the rapid rise, it is also true that

$$\frac{\rho}{\rho_a} = \frac{\ell_o}{H_s} \quad . \tag{21}$$

Solving (21) for $\ell_o$ and substituting $\ell_o$ into (20) yields

$$\frac{\rho}{\rho_a} = \left[1 + \frac{(\gamma-1)\varepsilon}{H_s p_a} \frac{\rho_a}{\rho}\right]^{-1/\gamma} \quad . \tag{22}$$

The transcendental Equation (22) can be solved for $\rho/\rho_a$ and hence the desired quantity,

$$\Delta\rho/\rho_a = 1 - \rho/\rho_a \quad . \tag{23}$$

## COMPARISON OF OBSERVATIONS TO BUOYANT EXPECTATIONS

Values of parameters for use in evaluation of (14), (15), (16), and (23) are

$g = 9.8$ m/sec$^2$, $f_r = 0.4$, $\gamma = 1.4$, and $p_a = .8 \times 10^6$ dynes/cm$^2$.

For Wasp Prime, $Y = 3.2$ kt , $h = 225$ m, $H_s \simeq 20$ m .

For Climax, $Y = 61$ kt , $h = 407$ m, $H_s \approx 50$ m .

Evaluations of pertinent quantities and comparisons to measurements are shown in Table 5. The coupling fraction, $f_c$, was varied from slightly less than the value Ganong and Whitaker chose to nearly twice their value.

Table 5. Buoyant predictions compared to data. The value of u shown for Wasp Prime is the average of those shown in Table 3 for the two values of $a/a_f$.

| Event | Feature | x(m) | R(m) | u(m/s) | $\varepsilon$(erg/cm$^2$) | $\Delta\rho/\rho$ | $u/\sqrt{Rg\Delta\rho/\rho}$ | $\Delta\rho/\rho$ | $u/\sqrt{Rg\Delta\rho/\rho}$ |
|---|---|---|---|---|---|---|---|---|---|
| Wasp Prime | 1 | -124 | 5.9 | 3.6 | $1.80\times10^9$ | .31 | .85 | .16 | 1.2 |
| | 2 | -80 | 4.4 | 5.2 | $2.36\times10^9$ | .38 | 1.3 | .20 | 1.8 |
| | 3 | 0 | 44 | 20 | $2.82\times10^9$ | .44 | 1.5 | .24 | 2.0 |
| | 4 | 131 | 5.9 | 4.2 | $1.82\times10^9$ | .30 | 1.0 | .16 | 1.4 |
| | 5 | 222 | 7.3 | 4.8 | $1.02\times10^9$ | .18 | 1.3 | .09 | 1.9 |
| Climax | 1 | -660 | 36 | 8.6 | $2.90\times10^9$ | .20 | 1.0 | .10 | 1.5 |
| | 2 | -350 | 55 | 12.7 | $7.15\times10^9$ | .45 | 0.82 | .24 | 1.1 |
| | 3 | 0 | 128 | 36.0 | $1.64\times10^{10}$ | .79 | 1.0 | .50 | 1.4 |
| | 4 | 800 | 30 | 8.0 | $1.53\times10^9$ | .11 | 1.4 | .05 | 2.1 |
| | | | | | | | $f_c = 0.30$ | | $f_c = 0.15$ |

Inspection of columns 8 and 10 in Table 5 shows that observed values of excess velocity, taken from Tables 3 and 4, fall within the range predicted by Equation 14. Thus, qualitatively and quantitatively, the data are consistent with buoyancy as the major driving force at late times, to the accuracy of measurements and within the confidence possible with an incomplete theory.

## SECTION 5
## PHENOMENA WHICH CANNOT LIFT DUST ADEQUATELY

This section presents a partial list of phenomena which might be suggested as candidates for raising dust to the early pedestal height, $H_s$, or for causing the late time pedestal rise. None of them singly can explain observations; in fact, it seems most unlikely that all of them in concert can explain either early pedestal rapid rise to $H_s$ or late slow rise. This is not to say that these phenomena are absent nor, as a member in some possible chain of events, unimportant. For example, popcorning is certainly real and may provide the dust, at a very low level, which a Hess bubble[9] or some other mechanism lifts to $H_s$, but popcorning itself does not raise dust as high as $H_s$.

### POPCORNING

This mechanism has been popular at least since the early 1950's. Basically, the mechanism consists of flash heating water laden material via bomb thermal, neutrons or gamms so severely that steam forms explosively causing dust to fly up into the air.

From (15) the maximum energy available at, say, $x = h$, is

$$M = \frac{f_c f_r W}{\sqrt{2}\ 8\pi h^2} \tag{23}$$

from bomb thermal; much less is available from gammas or neutrons.

Taking the energy necessary to raise water to the boiling point and convert it to steam as $I_s$, ergs/gm, the amount of steam possible is

$$m = \frac{f_c f_r W}{\sqrt{2}\ 8\pi I_s h^2} \quad . \tag{24}$$

Using Climax as an example and taking $f_r = 0.4$, $f_c = 1/3$, $I_s = 2.5 \times 10^{10}$ erg/gm.

$$m = 0.25 \text{ gram/cm}^2 \quad .$$

If this steam then expands to density comparable to ambient air, it will reach up to height

$$H_p = m/10^{-3} = 250 \text{ cm} = 2.5 \text{ m} \quad , \tag{25}$$

about a factor of 20 short of the required rise.

## STEAMING

Here one imagines the shock, perhaps with help from bomb thermal radiation, heating the ground and creating steam, or some other outgased product, at a rate slow compared to popcorning. Dust is presumed carried upward with the gas. Steaming fails on the same basis that popcorning fails; even less energy is available in the shock than in the thermal pulse.

## REVERSE PERCOLATION

In this process air is forced into soil cavities by the high pressure forward portion of the shock, then air plus soil is blasted upward when the pressure gradient reverses on the back side of the positive phase. Zernow and coworkers[10] have shown the process to be effective in lifting dessicated sand tens of centimeters under fairly realistic conditions. By "fairly" is meant a basically realistic pressure profile and hopefully realistic lower boundary condition (both are critical) but overoptimistic in that the material is: (1) dessicated, and (2) uncompacted.

Based upon their experiments, the process does not seem capable of raising dust more than a few meters at most. Further, their experiment showed the process to fail completely in very wet sand, whereas both Teapot 12 (Met) and Tumblers 1 through 4 show no effect on the dust pedestal of either artificial or natural wetting down of the shot region relative to dry desert surface.

## SUCTION

Suction is due to the rarefaction behind the shock and can be viewed as a continuation of reverse percolation. After the positive phase of the shock has passed, a rarefaction, typically a 20 percent reduction in atmospheric pressure, exists over a region similar in extent to the pedestal. If air at ambient pressure exists in soil interstitial regions it may be expelled and may carry some dust with it. Any rational perturbation of linear to nonlinear D'Arcy law interstitial flow yields only about a meter of air lifted by this mechanism.

## TURBULENCE

Turbulence has been suggested both as a mechanism for the initial pedestal rise and separately as a mechanism for the late rise.

As a mechanism to drive the early rapid rise turbulence seems not to withstand scrutiny on a rather basic level. In the most extreme case the shock proceeds outward and the pedestal proceeds upward at almost the same rate of speed. If the pedestal were rising as a consequence of some random process, which must be ultimately driven by the shock, it would rise with a $\sqrt{t}$ law, or rise some random fraction of the time—but could not rise always and steadily at a rate near that of shock propagation.

Turbulence as a driver of the late pedestal rise is not unlikely in principle, but it does not fit the observations. Of the nine pedestal features whose motions we followed (make it seven if one wishes to consider the sand columns to be special cases) all had excess velocities which were not only in the same general direction, a result most unlikely for a turbulent velocity field, but were quantitatively smooth and rather well predicted, a result nigh impossible in a random flow field.

## REFERENCES


1. Liner, R. T., et al., Nuclear Precursor Phenomenology and Sweep-up Dust Cloud Model, DNA 3781F, Science Applications, Inc., McLean, Virginia, 4 November 1975 (U).

2a. Dudziak, W. F., et al., Photographic Atlas Event WASP PRIME, DNA 3576F, 9 May 1975 (U).

2b. Dudziak, W. F., et al., Photographic Atlas of Event CLIMAX, Unpublished.

3. Gutsche, S. L., X-Band Attenuation from a Nuclear Dust Cloud Pedestal: Boundary Calculations and Determination of Sensitivity to Key Parameters, MRC-N-464, 15 May 1981 (U).

4. Lauer, C. J., Angle of Arrival Fluctuations in a Nuclear Dust Cloud Pedestal, MRC-N-476, August 1981 (U).

5. Thompson, James H., Preliminary Estimates of the Propagation Effects in a Nuclear Pedestal Region, Presentation at LoAD Dust Task Meeting, Defense Nuclear Agency, Washington, D.C., 11 March 1981 (U).

6. See Lamb's Hydrodynamics, Sixth Edition, Dover Press, p. 161, 214 or Physics of High Altitude Nuclear Burst Effects, DNA 4501F, p 480, December 1977 (U).

7. McCartor, G. D., and W. R. Wortman, Unpublished calculation, Mission Research Corporation.

8. Ganong, G. P., and W. A. Whitaker, The Nuclear Blast Precursor, AFWL-TR-69-199, Vol. 1, March 1969 (U).

9. Hess, R. V., Interaction of Moving Shocks and Hot Layers, Langley Aeronautical Laboratory, NACA Technical Note 4002, May 1957 (U).

10. Zernow, L., et al., An Experimental Study of the 'Reverse Percolation' Lofting Process in a Sand Medium, DNA 3210F, Shock Hydrodynamics Division of Whittaker Corporation, 16 November 1973 (U).

# DISTRIBUTION LIST

DEPARTMENT OF DEFENSE

Assistant Secretary of Defense
Comm, Cmd, Cont & Intell
ATTN: Dir of Intelligence Sys, J. Babcock

Command & Control Technical Ctr
Department of Defense
ATTN: C-312, R. Mason
ATTN: C-650, G. Jones
3 cy ATTN: C-650, W. Heidig

Defense Intelligence Agency
ATTN: Dir
ATTN: DB-4C, E. O'Farrell
ATTN: DB, A. Wise
ATTN: DT-1B
ATTN: DC-7B

Defense Nuclear Agency
ATTN: NAFD
ATTN: STNA
ATTN: RAEE
ATTN: NATD
4 cy ATTN: TITL
6 cy ATTN: RAAE

Defense Tech Info Ctr
12 cy ATTN: DD

Field Command
Defense Nuclear Agency
ATTN: FCPR, J. T. McDaniel

Field Command
Defense Nuclear Agency
Livermore Branch
ATTN: FCPRL

Interservice Nuclear Weapons School
ATTN: TTV

Under Secretary of Defense for Rsch & Engrg
Department of Defense
ATTN: Strategic & Space Sys (OS)

National Security Agency
ATTN: W-32, O. Bartlett
ATTN: B-3, F. Leonard
ATTN: R-52, J. Skillman

DEPARTMENT OF THE ARMY

Assistant Chief of Staff for Automation & Comm
Department of the Army
ATTN: DAAC-ZT, P. Kenny

Atmospheric Sciences Lab
U.S. Army Electronics R&D Command
ATTN: DELAS-EO, F. Niles

BMD Advanced Technology Ctr
Department of the Army
ATTN: ATC-O, W. Davies
ATTN: ATC-T, M. Capps

DEPARTMENT OF THE ARMY (Continued)

BMD Systems Command
Department of the Army
2 cy ATTN: BMDSC-HW

U.S. Army Communications R&D Command
ATTN: DRDCO-COM-RY, W. Kesselman

U.S. Army Comm-Elec Engrg Instal Agency
ATTN: CCC-CED-CCO, W.Neuendorf
ATTN: CCC-EMEO-PED, G. Lane

U.S. Army Foreign Science & Tech Ctr
ATTN: DRXST-SD

U.S. Army Materiel Dev & Readiness Cmd
ATTN: DRCLDC, J. Bender

U.S. Army Missile Intelligence Agency
ATTN: YSE, J. Gamble

U.S. Army Nuclear & Chemical Agency
ATTN: Lib

DEPARTMENT OF THE NAVY

Office of Naval Research
ATTN: Code 420
ATTN: Code 465
ATTN: Code 421

DEPARTMENT OF THE AIR FORCE

Air Force Geophysics Lab
ATTN: OPR, H. Gardiner
ATTN: OPR-1
ATTN: LKB, K. Champion
ATTN: OPR, A. Stair
ATTN: S. Basu
ATTN: PHP
ATTN: PHI, J. Buchau
ATTN: R. Thompson

Air Force Weapons Lab
Air Force Systems Command
ATTN: SUL
ATTN: NTYC
ATTN: NTN

Air University Lib
Department of the Air Force
ATTN: AUL-LSE

Space Division
Department of the Air Force
ATTN: SKA, D. Bolin
ATTN: SKY, C. Kennedy

Space Division
Department of the Air Force
ATTN: YGJB, W. Mercer

OTHER GOVERNMENT AGENCIES

Central Intelligence Agency
ATTN: OSWR/NED

Department of Commerce
National Bureau of Standards
ATTN: Sec Ofc for R. Moore

Department of Commerce
National Oceanic & Atmospheric Admin
ATTN: R. Grubb

Institute for Telecommunications Sciences
National Telecommunications & Info Admin
ATTN: W. Utlaut
ATTN: A. Jean
ATTN: L. Berry

DEPARTMENT OF ENERGY CONTRACTORS

Los Alamos National Lab
ATTN: P. Keaton
ATTN: R. Taschek
ATTN: G-6, E. Jones
ATTN: C. Westervelt
ATTN: D. Simons
ATTN: MS 664, J. Zinn
ATTN: MS 670, J. Hopkins

DEPARTMENT OF DEFENSE CONTRACTOR

Aerospace Corp
ATTN: T. Salmi
ATTN: J. Straus
ATTN: R. Slaughter
ATTN: V. Josephson
ATTN: I. Garfunkel
ATTN: D. Olsen
ATTN: N. Stockwell
ATTN: S. Bower

Analytical Systems Engineering Corp
ATTN: Radio Sciences

Analytical Systems Engineering Corp
ATTN: Security

Barry Research Corp
ATTN: J. McLaughlin

BDM Corp
ATTN: L. Jacobs
ATTN: T. Neighbors

Berkeley Research Associates, Inc
ATTN: J. Workman

BETAC
ATTN: J. Hirsch

Boeing Co
ATTN: M/S 42-33, J. Kennedy
ATTN: G. Hall
ATTN: S. Tashird

Booz-Allen & Hamilton, Inc
ATTN: B. Wilkinson

Communications Satellite Corp
ATTN: D. Fang

DEPARTMENT OF DEFENSE CONTRACTORS (Continued)

University of California at San Diego
Electrical Engineering Computer Sciences
ATTN: H. Booker

Charles Stark Draper Lab, Inc
ATTN: J. Gilmore
ATTN: D. Cox

Computer Sciences Corp
ATTN: F. Eisenbarth

Comsat Labs
ATTN: G. Hyde

Cornell University
Department of Electrical Engineering
ATTN: D. Farley, Jr
ATTN: M. Kelly

E-Systems, Inc
Center for Planning & Analysis
ATTN: R. Berezdivin

Electrospace Systems, Inc
ATTN: H. Logston

ESL, Inc
ATTN: J. Marshall

General Electric Co
ATTN: A. Harcar

General Electric Co
ATTN: A. Steinmayer
ATTN: C. Zierdt

General Electric Co
ATTN: F. Reibert

General Electric Co
ATTN: G. Millman

General Research Corp
ATTN: J. Ise, Jr
ATTN: J. Garbarino

Harris Corp
ATTN: E. Knick

Horizons Technology, Inc
ATTN: R. Kruger

HSS, Inc
ATTN: D. Hansen

IBM Corp
ATTN: F. Ricci

University of Illinois
ATTN: Security Supr for K. Yeh

Institute for Defense Analyses
ATTN: J. Aein
ATTN: H. Gates
ATTN: H. Wolfhard
ATTN: E. Bauer

JAYCOR
ATTN: J. Sperling

DEPARTMENT OF DEFENSE CONTRACTORS (Continued)

International Tel & Telegraph Corp
ATTN: W. Rice
ATTN: Tech Lib

JAYCOR
ATTN: J. DonCarlos

Johns Hopkins University
ATTN: T. Potemra
ATTN: J. Phillips
ATTN: T. Evans
ATTN: J. Newland
ATTN: P. Komiske

Kaman Tempo
ATTN: T. Stephens
ATTN: DASIAC
ATTN: W. McNamara
ATTN: W. Knapp

Linkabit Corp
ATTN: I. Jacobs

Litton Systems, Inc
ATTN: R. Grasty

Lockheed Missiles & Space Co, Inc
ATTN: R. Johnson
ATTN: W. Imhof
ATTN: M. Walt

Lockheed Missiles & Space Co, Inc
ATTN: Dept 60-12
ATTN: D. Churchill
ATTN. C. Old

M.I.T. Lincoln Lab
ATTN: D. Towle

Martin Marietta Corp
ATTN: R. Heffner

McDonnell Douglas Corp
ATTN: J. Moule
ATTN: G. Mroz
ATTN: W. Olson
ATTN: N. Harris
ATTN: R. Halprin

Meteor Communications Consultants
ATTN: R. Leader

Mission Research Corp
ATTN: S. Gutsche
ATTN: R. Bogusch
ATTN: D. Sappenfield
ATTN: F. Fajen
ATTN: Tech Lib
ATTN: R. Hendrick
ATTN: R. Kilb
4 cy ATTN: D. Sowle
4 cy ATTN: R. Christian
5 cy ATTN: Doc Con

Mitre Corp
ATTN: A. Kymmel
ATTN: C. Callahan
ATTN: G. Harding
ATTN: B. Adams

DEPARTMENT OF DEFENSE CONTRACTORS (Continued)

Mitre Corp
ATTN: M. Horrocks
ATTN: J. Wheeler
ATTN: W. Hall
ATTN: W. Foster

Pacific-Sierra Research Corp
ATTN: E. Field, Jr
ATTN: F. Thomas
ATTN: H. Brode

Pennsylvania State University
ATTN: Ionospheric Research Lab

Photometrics, Inc
ATTN: I. Kofsky

Physical Dynamics, Inc
ATTN: E. Fremouw

Physical Research, Inc
ATTN: R. Deliberis

R & D Associates
ATTN: R. Lelevier
ATTN: R. Turco
ATTN: H. Ory
ATTN: B. Gabbard
ATTN: M. Gantsweg
ATTN: W. Wright
ATTN: C. Greifinger
ATTN: W. Karzas
ATTN: F. Gilmore
ATTN: P. Haas

R & D Associates
ATTN: B. Yoon

Rand Corp
ATTN: E. Bedrozian
ATTN: C. Crain

Riverside Research Institute
ATTN: V. Trapani

Rockwell International Corp
ATTN: R. Buckner

Rockwell International Corp
ATTN: S. Quilici

Santa Fe Corp
ATTN: D. Paolucci

Science Applications, Inc
ATTN: L. Linson
ATTN: D. Hamlin
ATTN: E. Straker
ATTN: C. Smith

Science Applications, Inc
ATTN: SZ

Science Applications, Inc
ATTN: J. Cockayne

Technology International Corp
ATTN: W. Boquist

DEPARTMENT OF DEFENSE CONTRACTORS (Continued)

SRI International
ATTN: W. Chesnut
ATTN: R. Leadabrand
ATTN: D. Neilson
ATTN: J. Petrickes
ATTN: R. Livingston
ATTN: G. Price
ATTN: W. Jaye
ATTN: C. Rino
ATTN: A. Burns
ATTN: R. Tsunoda
ATTN: G. Smith
ATTN: M. Baron

Sylvania Systems Group
ATTN: R. Steinhoff
ATTN: I. Kohlberg
ATTN: J. Concordia

DEPARTMENT OF DEFENSE CONTRACTORS (Continued)

Tri-Com, Inc
ATTN: D. Murray

TRW Defense & Space Sys Group
ATTN: R. Plebuch
ATTN: D. Dee

Utah State University
ATTN: K. Baker
ATTN: J. Dupnik
ATTN: L. Jensen

Visidyne, Inc
ATTN: C. Humphreys
ATTN: J. Carpenter